Nanoscale Advances

ROYAL SOCIETY OF CHEMISTRY

PAPER

View Article Online
View Journal | View Issue

Cite this: *Nanoscale Adv.*, 2025, **7**, 2626

A nitrogen and phosphorus enriched inorganic–organic hybrid material for electrochemical detection of selenium(IV) ions†

Arun Kumar, ‡ Prakriti Thakur, ‡ Nisha Dhiman, Sachin Balhara and Paritosh Mohanty *

A heteroatom (nitrogen and phosphorus) enriched pyridinic bridged inorganic–organic hybrid material (HPHM) was synthesized by polycondensing phosphonitrilic chloride trimer (PNC) and 2,6-diaminopyridine in DMSO at 140 °C. The synthesized material was used as an efficient electrode material for the electrochemical detection of selenium(IV) ions [Se(IV)] in aqueous solution. The HPHM electrode (active mass loading of 4.1 mg cm^{-2}) achieves a detection range of 5–50 ppb at a deposition potential of −1.2 V and a deposition time of 170 s with a lower limit of detection (LOD) of 2.18 ppb. This LOD is significantly below the World Health Organization's (WHO) recommended maximum level for selenium in drinking water. Moreover, the electrode material maintains high selectivity for Se(IV) ions in the presence of various interfering ions and high sensitivity over 200 cycles with only a minimal (~6.83%) decline in current density response. The higher Se(IV) ion detection capability is attributed to the strategic incorporation of nitrogen and phosphorus heteroatoms, enhancing the material's electrochemical properties.

Received 21st January 2025
Accepted 5th March 2025

DOI: 10.1039/d5na00079c

rsc.li/nanoscale-advances

1. Introduction

Selenium (Se) is a non-metallic element that can be sporadically found in about 0.05 to 0.2 mg kg^{-1} in the Earth's crust.[1] It predominantly exists in its elemental form or as a constituent of pure ore complexes.[2–4] Notably, it is a significant environmental pollutant, commonly found in various metallic ores and sulphide minerals.[4,5] Both natural occurrences, such as the weathering of Se-containing rocks and volcanic explosions, along with some anthropogenic activities, such as the mining of seleniferous ores and the burning of fossil fuels, contribute to its atmospheric release in the form of selenide (H_2Se), selenate (SeO_4^{2-}), selenite (SeO_3^{2-}), *etc.* Selenium can quickly accumulate in food chains, making it a potential hazard to aquatic organisms and the environment.[6] This dual impact from natural and anthropogenic sources underscores the urgency of understanding and mitigating selenium pollution.[7–10] The different valence states of selenium are elemental selenium (Se^0), selenide (Se^{2-}), selenite [Se(IV), SeO_3^{2-}], and selenate [Se(VI), SeO_4^{2-}]. Se(IV) and Se(VI) are the most prevalent forms in water bodies. Among the different forms of selenium, Se(IV) is the most hazardous and the sole electroactive form.[9–13] In an acidic environment, Se(IV) gets reduced to selenium (Se) and selenium hydride (H_2Se), using 10 H^+ and 10 e^-. The H_2Se further reacts with sodium selenate (Na_2SeO_3) *via* a comproportionation reaction, leading to the production of red selenium (Se).[11,12,14] Selenium is also a micronutrient found in numerous enzymes, such as selenocysteine (modified amino acid), whose moderate amounts are essential for human well-being.[15–21] It is a constituent of glutathione peroxidase (GSHPx), peroxidase, and thioredoxin reductases, which prevent oxidative damage of tissues, assist in thyroid hormone metabolism, and break intramolecular disulphide bonds.[22–26] However, excessive selenium intake can lead to selenosis, resulting in adverse health effects. The interaction of selenium with thiols can disrupt the activity of DNA and cause toxicity. Symptoms of selenium poisoning include lung congestion, gastrointestinal issues, changes in nail and hair structure, and other structural abnormalities.[26–30]

Recognizing the potential dangers associated with elevated selenium levels, the World Health Organization (WHO) has established a permissible limit of 10 and 40 parts per billion (ppb) for selenium in drinking and groundwater, respectively.[31] Therefore, it is essential to perform precise, selective, on-the-spot detection of selenium in different environmental matrices, such as sources of drinking water, groundwater, and rivers.[26] Various characterization techniques are available for quantifying the selenium concentration, such as flame absorption spectroscopy (FAAS, 10–8200 mg L^{-1}) and graphite

Functional Materials Laboratory, Department of Chemistry, Indian Institute of Technology (IIT) Roorkee, Roorkee, Uttarakhand-247667, India. E-mail: paritosh75@gmail.com; pm@cy.iitr.ac.in

† Electronic supplementary information (ESI) available. See DOI: https://doi.org/10.1039/d5na00079c

‡ Both authors have equal contribution.

furnace atomic absorption spectroscopy (GFAAS, 0–50 μg L^{-1}). However, each method has its own limitations, such as sensitivity, response time, and narrow range of linear response.[21,32] The more advanced inductively coupled plasma mass spectrometry (ICP-MS, 0.1 μg L^{-1}) has a very high sensitivity[32–36] but is associated with an operational cost. Moreover, these methods involve the requirement of initial preparatory steps, the use of premium reagents and standards, reliance on skilled workers, labor-intensive sample preparation, and processing procedures. These limitations also limit their use in lab settings and make it more challenging to automate them for routine, on-site, and real-time assessments of Se(IV) ions in water bodies. Additionally, during different phases of sample collection, transit, storage, and preparation, the physicochemical properties of the samples may also be compromised. Electroanalytical methodologies such as square wave voltammetry (SWV), adsorptive cathodic stripping voltammetry (CSV), anodic stripping voltammetry (ASV), and differential pulse voltammetry (DPV) have been explored as alternatives. These methods have several advantages, such as simple instrumentation, the possibility of downsizing, portability, ease of use, and speedy analysis.[37–39] Nonetheless, the analytical properties of the electrode or sensor material have a significant impact on the efficacy of these electroanalytical methods.

Several metal-based electrochemical sensors have been utilized for selenium detection, such as modified electrodes made up of bismuth and mercury and macro-electrodes made up of Hg, Pt, Ag, Au, *etc.*, to attain the desired levels of cost-effectiveness, reproducibility, sensitivity, and selectivity.[26,40,41] Rodrigo *et al.*[42] reported electrochemical detection of Se(IV) using glassy carbon electrode modified with Au nanoparticles and the LOD was found to be 120 ppb. However, metal-free sensors ought to be utilized to eliminate the environmental issues associated with the leaching of metal from the metal-based electrodes in the electrochemical sensor. Tanaka *et al.* used diamino naphthalene (DAN) for modification of the electrochemical sensor surface for the detection of selenium due to the chelation of the nitrogen atom of DAN with Se(IV) with a limit of detection (LOD) of 0.788 ppb.[43] Further, Ashournia *et al.* employed TMF/GCE in an acidic environment to detect selenium utilizing 4-nitro-1,2-phenylenediamine (NoPD).[44] A complex named 5-nitropiazselenol was formed between the selenium(IV) and nitrogen atoms of 4-nitro-1,2-phenylenediamine (NoPD). Selenium(IV) was effectively detected in natural water samples up to 0.06 ppb using this method.[44] Thus, the development of effective heteroatom enriched materials which have higher complex forming ability with selenium is essential.

Heteroatoms like oxygen, sulphur, and nitrogen have a specific ability to chelate, which makes the modifier-based electrodes that contain some heteroatom ligands a suitable complexing agent for detecting trace elements.[45–49] Therefore, a heteroatom-enriched (N and P) material denoted as HPHM[50] has been synthesized by a conventional heating method using 2,6-diaminopyridine and phosphonitrilic chloride and used for electrochemical detection of Se(IV) ions. The active mass loading, deposition potential (DP), deposition time (DT), and concentration were optimized to design an electrochemical sensor with enhanced performance for Se(IV) ion detection.

2. Experimental section

2.1. Materials

Phosphonitrilic chloride trimer (PNC, $Cl_6N_3P_3$, 99% Sigma-Aldrich, UK), 2,6-diaminopyridine (DAP, $C_5H_7N_3$, 98% Alfa Aesar, India) and dimethyl sulfoxide (DMSO, C_2H_6SO, SRL, India) are used for the synthesis of HPHM. Sodium selenite (Na_2SeO_3, 99% Avra Synthesis Pvt. Ltd, India) was used to prepare the stock solution (1 mM) of Se(IV) ions. Nitric acid (HNO_3, 99%, Rankem) was used as the supporting electrolyte. The active electrode material coated on a graphite sheet (~0.1 mm thickness, Nickunj Eximp Emtp. India) was used as a current collector. Polyvinylidene fluoride (PVDF), *N*-methylpyrrolidone (NMP, C_5H_9NO, 99%, HiMedia Laboratories Pvt. Ltd), and activated carbon (AC, Super P, Alfa Aesa, India) were used for the preparation of the active electrode material.

2.2. Synthesis of HPHM

The synthesis of HPHM was carried out using polycondensation of PNC and DAP, as per our previous report.[47,50] The reaction has been carried out by conventionally heating the precursors dissolved in DMSO at 140 °C for 18 h. The detailed synthesis procedure is provided in the ESI.†

2.3. Fabrication of electrodes for electrochemical investigations

The HPHM was used as an active material for the fabrication of electrodes for electrochemical detection of Se(IV) ions. To prepare the HPHM electrode, 3 mg of PVDF was dissolved completely in 150 μL of NMP in a 5 mL culture tube. In a mortar and pestle, 3 mg of AC was ground properly with 14 mg of HPHM. The powdered mixture was then transferred into the culture tube containing PVDF dissolved in NMP. The resulting dispersion was stirred for 48 h at RT to get a homogeneous mixture, which was uniformly drop-casted on a graphite sheet (1×1 cm^2). The fabricated electrode was finally kept in a hot air oven for 12 h at 60 °C before employing it for electrochemical studies.

2.4. Electrochemical measurements

A three-electrode cell configuration was utilized for the electrochemical detection of Se(IV) ions. Ag/AgCl was used as the reference electrode, and Pt wire was used as the counter electrode. The fabricated HPHM electrode of 1×1 cm^2 was used as a working electrode (Fig. 1). To evaluate the electrochemical performance of the electrode, cyclic voltammetry (CV) and electrochemical impedance spectroscopy (EIS) were performed. A solution of 0.1 M nitric acid (HNO_3) containing 0.1 M $[Fe(CN)_6]^{3-/4-}$ was used for the electrochemical measurements. The CV was scanned from −0.2 to 0.8 V from 5 to 100 mV s^{-1}. The EIS was performed from 0.1 to 10^5 Hz at an amplitude of the applied potential of 10 mV. To examine the response for the Se(IV) ion sensing, differential pulse voltammetry (DPV) was

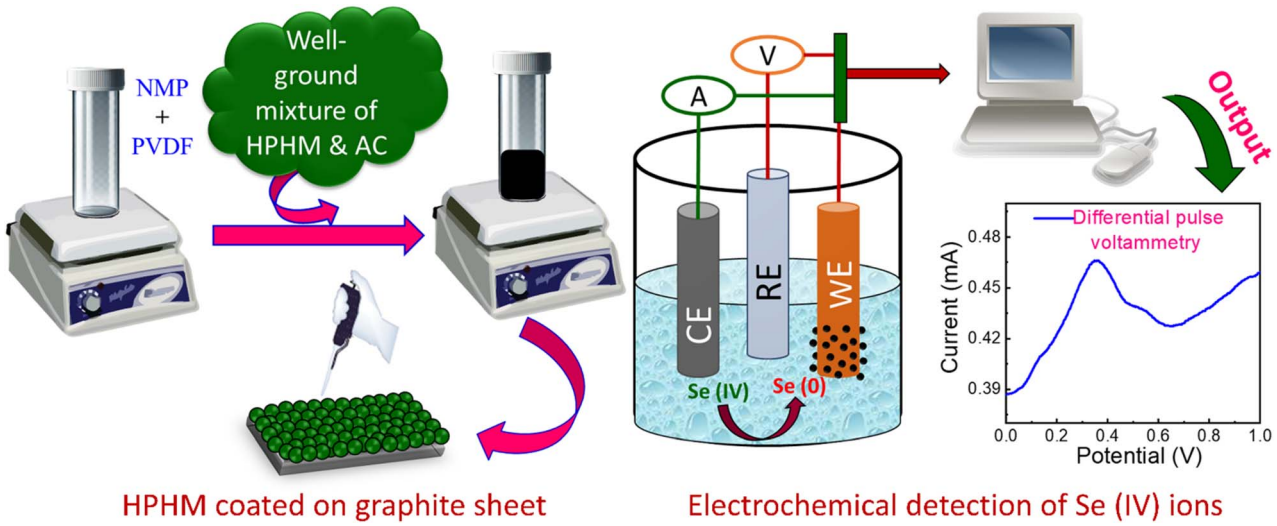

Fig. 1 Schematic representation of the electrochemical setup for the detection of Se(IV) ions.

conducted under specific sensing parameters *viz.*, deposition potential (DP) of −1.2 V, deposition time (DT) of 170 s at 10 mV s^{-1}. A supporting electrolyte of 0.1 M HNO_3 was used for electrochemical measurements. A Multi Autolab/M204 electrochemical workstation (Metrohm Autolab B.V., Netherlands) was used to carry out all electrochemical measurements. The limit of detection (LOD) was calculated using the following equation:

$$\mathrm{LOD} = 3.3 \times (\mathrm{SD}/m) \quad (1)$$

where SD = standard deviation of the intercept and m = the slope of the curve. Furthermore, the HPHM electrode was used to detect the Se(IV) ions in the tap water sample.

3. Results and discussion

3.1. Structural, microstructural and textural characterizations

The successful synthesis of HPHM[47,50] was confirmed by state-of-the-art characterization techniques such as FT-IR, XRD, FESEM, TEM, and N_2 sorption measurements. The FT-IR spectra of the HPHM, along with the reactants, *i.e.*, DAP and PNC, are given in Fig. S1a.† The observation of a broad band in HPHM around 3400 cm^{-1} instead of multiple bands between 3116 and 3405 cm^{-1} of the primary amine, as seen in the DAP, confirms the polymerization (Fig. S1a†).[47,48,50] The stretching frequencies of pyridine rings are also observed in HPHM near 1600 [*vs.* (C=N)], 1570 [*vs.* (C=C)], and 1290 cm^{-1} [*vs.* (C–N)]. Additionally, stretching frequencies near 1370 and 1220 cm^{-1} [*vs.* P=N–P], 1000–960 cm^{-1} [*vs.* (P=NH–C)], and 860 cm^{-1} [P–N ring vibrations] confirm the presence of cyclophosphazene moieties in HPHM.[47,48,50] Importantly, the absence of the P–Cl band in HPHM (600–500 cm^{-1}) shows the successful condensation of DAP and PNC to form the polymeric framework.[50]

Furthermore, X-ray diffraction (XRD) analysis of HPHM exhibited a broad halo indicating the amorphous nature of the material as shown in Fig. S1b.† The textural properties were analyzed by N_2 sorption analysis measured at 77 K (−196 °C). The N_2 sorption isotherm is shown in Fig. S2a.† A type-II isotherm could be seen with very little uptake at the low-pressure region. The estimated specific surface area using the BET equation (SA_{BET}) was found to be 7 m^2 g^{-1}. The BET plot is shown in the Fig. S2b† inset. The pore size distribution (PSD), estimated by density functional theory with kernel "N_2 at 77 K on carbon: Slit Pores, QSDFT equilibrium model", shows that predominant pores are centered at 1.8 nm, with the tail extended for multimodal PSD (Fig. S2b†). A total pore volume of 0.016 cm^3 g^{-1} was estimated at a relative pressure (P/P_o) of 0.99. Microstructural analysis of the HPHM was performed by FESEM and TEM (Fig. S3a and b†). A non-uniform microstructure of the HPHM with various shapes and sizes was observed from FESEM, as shown in Fig. S3a.† Moreover, the TEM image of the HPHM reveals that different sizes of pores ranging from 5 to 20 nm were present (Fig. S3b†), which was also confirmed by the PSD from N_2 sorption measurements (Fig. S2b†). The selected-area electron diffraction pattern (SAED) (Inset Fig. S3b†) of the HPHM represents the amorphous nature of the specimen, which further corroborated the XRD findings (Fig. S1b†).

3.2. Electrochemical characterizations

The electrochemical properties of the HPHM electrode in 0.1 M HNO_3 with $[Fe(CN)_6]^{3-/4-}$ were studied using cyclic voltammetry (CV). The CV curves of the HPHM electrode were plotted at various scan rates ranging from 5 to 100 mV s^{-1}, as shown in Fig. 2a. It was observed that the peak current (i_p) increased gradually with an increase in the scan rate. Furthermore, the i_p of both anodic and cathodic peaks was linearly dependent on the square root of the scan rate, and their respective correlation coefficient was calculated (Fig. 2b). The R^2 for HPHM at the anodic (i_{pa}) region and cathodic region (i_{pc}) was found to be 0.99027 and 0.9881, respectively. This demonstrated that a diffusion-controlled mass transfer process occurred at the interface of the HPHM electrode. The electrochemical active

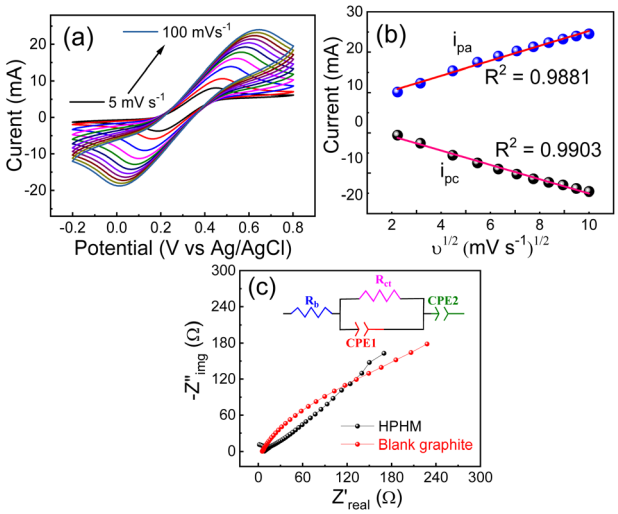

Fig. 2 (a) CV of HPHM electrodes from 5 to 100 mV s^{-1} in 0.1 M HNO_3 solution containing 0.1 M $[Fe(CN)_6]^{3-/4-}$, (b) the linear relationship between the redox peak current and square root of scan rate, (c) EIS spectra of the HPHM and blank graphite electrode.

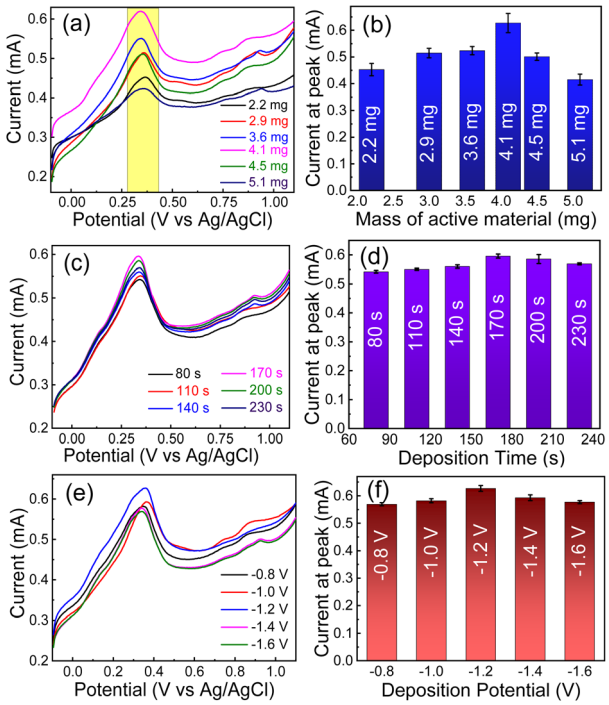

Fig. 3 (a) DPV response of Se(IV) with electrodes having different active material masses at 10 mV s^{-1} (b) The effect of the mass of the active material on the detection of Se(IV), (c) and (d) optimization of the DP, and (e) and (f) optimization of DT with standard deviation. (DT = 170 s, DP = −1.2 V, mass loading = 4.1 mg).

surface area (EASA) of the electrode materials can have a significant impact on the electrochemical performance. Therefore, EASA was calculated, and it was found to be 0.1 cm^2 for the HPHM electrode. Furthermore, EIS was performed to investigate the interfacial properties of the HPHM electrode and compare it with a blank graphite sheet electrode (Fig. 2c). The charge transfer resistance for the HPHM electrode was found to be ~6.32 Ω. A lower bulk resistance (R_b) of ~1.5 Ω was observed in the case of HPHM than for the blank graphite sheet (~5.3 Ω) which indicates better interfacial kinetics of HPHM. The diffusion coefficient was also calculated from the EIS (eqn (3)) and found to be 1.66 × 10^{-10} cm^2 s^{-1}, indicating a slow diffusion of the electroactive species.

Although HPHM possesses a low surface area, the presence of heteroatoms (nitrogen and phosphorus) in its polymeric framework, as well as its high electrochemically active surface area (EASA), makes HPHM a promising electrode material for detecting selenium(IV) ions. The electrochemical detection of the Se(IV) ion was performed using DPV in the potential range of −0.1 to 1.1 V at 10 mV s^{-1} in 0.1 M HNO_3 electrolyte. All the electrochemical detection experiments were repeated four times to get the reproducibility of the detection measurements. Initially, the electrodes of HPHM were fabricated by varying the mass of the active material, and DPV was subsequently measured.

As shown in Fig. 3a, the observation of a sharp peak at 0.32 V in all the DPVs indicated the electrochemical detection of the Se(IV) ions. Se(IV) ions present in the acidic medium were reduced to Se and H_2Se by following the two pathways when the potential was applied to it, as per eqn (2) and (3).[51,52] The reduction of Se(IV) occurs at potentials ranging from 0.25 to 0.4 V (*vs.* Ag/AgCl). Further, as the potential is increased, the formation of H_2Se takes place [eqn (3) and (4)]. In the acidic medium, H_2Se can react with Na_2SeO_3 to undergo a comproportionation reaction [eqn (5)].[51,52] This reaction leads to the formation of red selenium, which is a substance that has distinct red coloration.[51,52] The electrochemical reduction of Se(IV) ions is represented as follows:

$$Na_2SeO_3 + 4H^+ + 4e^- \rightarrow Se + H_2O + 2NaOH \quad (2)$$

$$Na_2SeO_3 + 6H^+ + 6e^- \rightarrow H_2Se + H_2O + 2NaOH \quad (3)$$

$$Se + 2H^+ + 2e^- \rightarrow H_2Se \quad (4)$$

$$Na_2SeO_3 + 2H_2Se \rightarrow 3Se\ (Red) + H_2O + 2NaOH \quad (5)$$

3.3. Optimization of the electrochemical measurement

To determine the ideal mass loading for the efficient sensing of selenium, electrodes of dimensions 1 × 1 cm^2 were fabricated using HPHM active mass loadings of 2.2, 2.9, 3.6, 4.1, 4.5, and 5.1 mg, keeping all other fabrication conditions identical. These electrodes are utilized at a fixed potential of 0.32 V. The current response increased with an increase in mass loading until it reached a maximum value of 0.62 mA at a mass loading of 4.1 mg, and afterward, it began to decrease with further increase in the mass loading (Fig. 3a and b). The initial current response increases up to the electrode mass of 4.1 mg due to an increase in the overall active mass, which provides a greater number of active sites for the electrochemical reaction to occur and effective electron transfer between the active electrode material and

the current collector. This leads to an increase in the probability of extensive interaction between a substantial portion of the electrode material with the current collector and the analyte.[53,54] Therefore, it can lead to a more significant number of electrons being transferred and, hence, a higher current response. However, decreases in the current response at a higher mass loading could be attributed to the additional particles of the active material hindering the analyte's access to all the active sites and increasing the resistance for electron transfer from the electrode material to the current collector.[50,55] Therefore, 4.1 mg was selected as the optimized mass of the HPHM electrode for Se(IV) ion detection. This further suggests that the active mass loading of the electrode plays a crucial role and significantly impacts the electrochemical performance.

DT is also an important parameter. The current response was measured by varying the DT from 80 to 230 s at a constant DP of −1.2 V (Fig. 3c). The current response trend is similar to the trend observed in the variation of the active mass loading. A maximum response current of 0.6 mA was observed at 170 s (Fig. 3d). The increase in peak current occurred because a longer DT allowed for more contact between the electrode surface and the electroactive species in the electrolyte.[56] As a result, the reaction rate was increased, and a higher number of Se(IV) ions started to accumulate at the electrode surface.[57,58] However, a further increase in the DT led to a decrease in the current due to the saturation of the analyte species on the electrode surface or the microstructural changes affecting electron transfer, and further deposition could not contribute to an increase in current.[59,60] The FESEM image of the electrode surface beyond 170 s shows significant changes in the microstructure of the electrode surface (Fig. S4c and d†). The electrode surface exhibited a flocculent (fluffy) microstructure with agglomerated particles, indicating the excessive accumulation of selenium. Therefore, 170 s was selected as the optimized DT for Se(IV) ion detection by the HPHM electrode. To obtain an optimal electrochemical response for Se(IV) ion sensing, the DP was varied, keeping all other experimental conditions identical (Fig. 3e). With an increase in the potential from −0.8 to −1.2 V, there was an increase in the response current from 0.57 to 0.63 mA. On further increase in the DP, the current was decreased (Fig. 3f).

The increase in current can be explained by a faster rate of electron transfer at the interface of the electrodes and the electrolyte. As the DP increased up to −1.2 V, there was an increase in the reaction rate, because of which more Se(IV) ions started to accumulate at the surface of the electrode. Therefore, the observed increase in the response current can be explained by the combined effect of faster electron transfer and the accumulation of Se(IV) ions on the HPHM electrode surface.[47,50,61] On further increasing the DP beyond −1.2 V, the response current began to decrease. This could be attributed to the formation of a barrier in the flow of the current due to the saturation of the electrode surface.[48,62] As a result, the access of the ions to the active sites was now limited, causing a decline in the response current. Moreover, a higher negative potential also causes structural changes on the fabricated electrode surface (Fig. S4e and f†).[48] At higher potential, water splitting led to evolution of H_2 gas at the electrode which led to the swelling of the graphite sheet. In fact, the evolution of gas could detach the active material from the current collector (graphite sheet) which can diminish the electrochemical performance. Further, FESEM analysis of the electrode surface was carried out after the DP of −1.4 V. FESEM analysis reveals the change in the microstructure of the electrode surface, where agglomerated selenium particles can be seen (Fig. S4e and f†). Keeping all of this in mind, −1.2 V was chosen as the optimized DP.

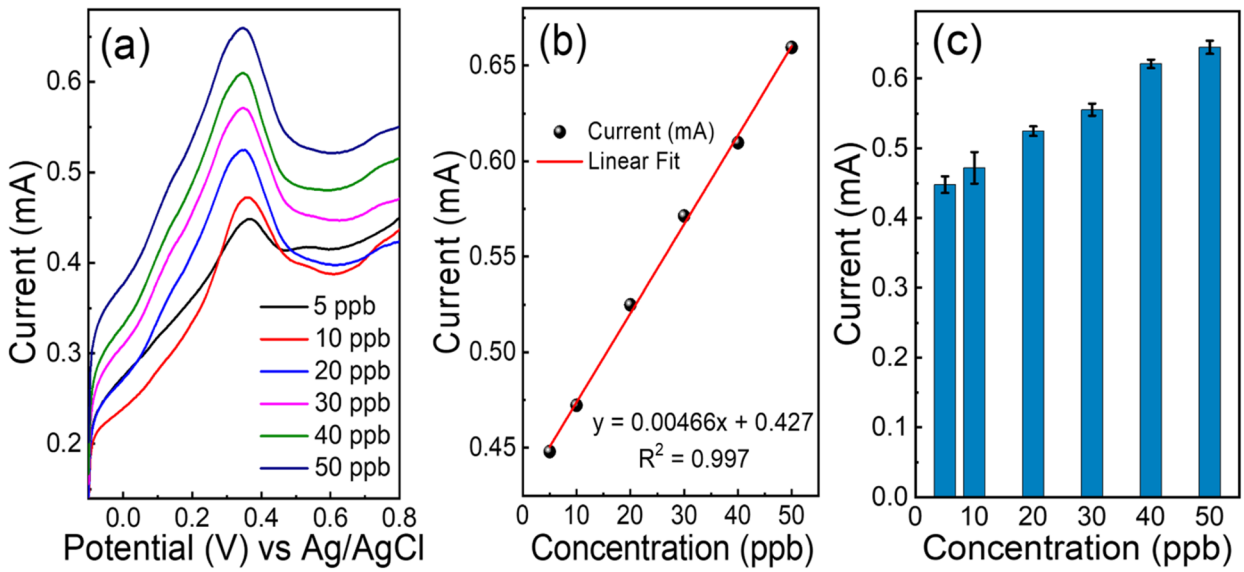

Fig. 4 (a) DPV response of increasing Se(IV) concentration on the HPHM electrode (b) calibration curve for Se(IV) at different concentrations (scan rate = 10 mV s^{-1}, DP = −1.2 V, DT = 170 s and mass of active material = 4.1 mg) and (c) repeatability towards detection of the Se(IV) ions.

The Se(IV) ion concentration in 0.1 M HNO_3 was varied from 5 to 50 ppb, and the response current was measured at 170 s (Fig. 4a). The current at the peak rises linearly up to 50 ppb with the peak linear regression's correlation value found to be 0.997 indicating a better linear relationship between current and concentration (Fig. 4b). Moreover, the limit of detection of HPHM was calculated using eqn (1) and found to be 2.18 ppb. The obtained lower LOD indicates the high performance of the HPHM, which can be a highly valuable sensor for the electrochemical detection of Se(IV) ions. Each of the experiments was carried out four times to improve the reproducibility of the results. To ensure the reproducibility of the HPHM electrode, five separate electrodes were fabricated with the same mass loading. Each electrode was subjected to five cycles at 10 mV s^{-1} (Fig. 5a). The RSD value was found to be 4.1%. This observation indicates that the HPHM electrode as an electrochemical sensor for Se(IV) ions is highly reproducible. Furthermore, to access the reusability of the HPHM electrodes for prolonged cycles, DPV was conducted for up to 200 cycles (Fig. 5b) and the RSD value was found to be 3.9%, further validating the HPHM's long-term stability and reusability. The polymeric framework of HPHM, enriched with heteroatoms such as N and P, plays a significant role in maintaining stability and preventing degradation. The presence N and P enhances the electrochemical performance and selectivity towards detection of Se(IV) ions. Moreover, there is negligible interference from common ions (this has been confirmed in the interference study, as discussed later), suggesting the electrode material resists contamination and fouling, which contributes to its high stability. The electrode maintained its structural stability over extended use, as only ~6.83% fading in current was observed even after 200 cycles, indicating the robust nature of the material (Fig. 5b). The obtained results demonstrated that the developed electrochemical sensor HPHM provides excellent performance in terms of reproducibility and reusability. However, FESEM analysis after 200 cycles revealed microstructural changes, with agglomerated selenium particles deposited on the surface of the electrode after repeated cycles (Fig. S4g and h†).

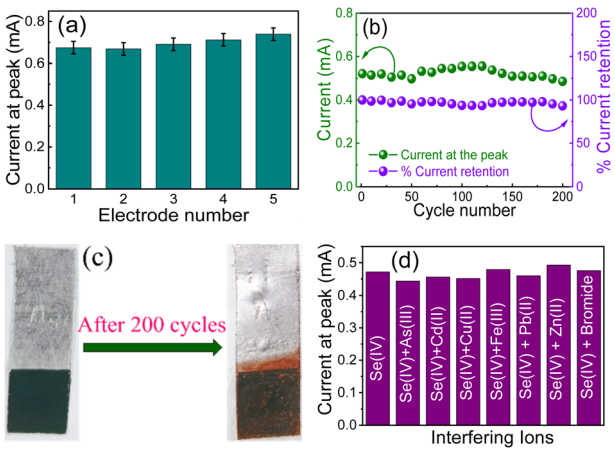

Fig. 5 (a) Reproducibility, (b) reusability of the HPHM electrode, (c) photographs of the electrode before and after the experiment, and (d) DPV response of 10 ppb Se(IV) ions in the presence of various interfering ions (100 ppb).

3.4. Effect of interfering ions

The effectiveness of the HPHM electrode in detecting Se(IV) ions in the presence of other commonly found interfering ions in water has been investigated. To achieve this, various cations such as Fe(III), Cu(II), Zn(II), As(III), Cd(II), and Pb(II), and an anion (Br^-) were studied at a higher concentration of interfering ions (100 ppb) under optimized conditions (Fig. 5d). The results revealed that the current response remained almost identical for the high concentrations of Fe(III) and Zn(II), indicating the high selectivity of Se(IV) ions even in the presence of both cations. However, a slight decrease in the detection current response was observed in the presence of 100 ppb of As(III), Cd(II), Cu(II), and Pb(II), indicating that these ions may interfere in the detection of Se(IV) ions. However, it is worth mentioning that this amount of different cation concentrations along with Se(IV) in real water samples is negligible. Therefore, the HPHM electrode can effectively detect the Se(IV) in real water samples.

3.5. Se(IV) detection in tap water

Applicability of HPHM for Se detection has been further extended to evaluation using 10 ppb Se(IV) (corresponding to the allowed limit in drinking water as set by WHO) in tap water. Additionally, a control experiment was also conducted to compare using tap water without adding Se(IV) salt. The former has exhibited a peak in DPV curve indicating successful detection of Se(IV) (Fig. S5†), while the latter specimen did not show any detectable peak, indicating the absence of Se(IV) in tap water at measurable levels.

4. Conclusion

A heteroatom (N and P) enriched pyridinic bridged inorganic–organic hybrid material (HPHM) was synthesized by a conventional polycondensation method. The synthesized HPHM was explored for the electrochemical sensor to detect toxic Se(IV) ions. The electrodes fabricated using HPHM as the active material were highly efficient towards electrochemical detection of Se(IV) ions owing to the presence of heteroatoms (N and P) in the polymeric framework. The optimized conditions for Se(IV) detection were an active mass loading of 4.1 mg cm^{-2}, DP of −1.2 V, and DT of 170 s. Under optimized conditions, the HPHM electrode could detect Se(IV) ions at concentrations of 5 to 50 ppb with a lower value of the limit of detection (LOD) of 2.18 ppb. In the present study, the LOD achieved by the HPHM was far below the allowed limit set by the WHO. Only ~6.83% fading in the current was observed after 200 cycles indicating the higher stability of the electrode material towards Se(IV) ion detection. Additionally, the HPHM electrode material was found to be highly selective, showing negligible interference from other ionic species in real water. These findings suggest that HPHM can act as an excellent, highly durable, and highly selective electrochemical sensor for Se(IV) ion detection.

Data availability

The data supporting this article have been included as part of the ESI.†

Author contributions

AK: investigation, methodology, project administration, validation, visualization, writing – original draft, writing – review & editing; PT: investigation, methodology, validation, visualization, writing – review & editing; ND: data curation, formal analysis; SB: formal analysis; PM: conceptualization, funding, investigation, project administration, supervision, writing – review & editing.

Conflicts of interest

There are no conflicts to declare.

Acknowledgements

AK acknowledges an SRF fellowship from UGC, Govt. of India.

References

1 V. Funari, H. I. Gomes, D. Coppola, G. A. Vitale, E. Dinelli, D. de Pascale and M. Rovere, *Resour. Conserv. Recycl.*, 2021, **170**, 105593.
2 C. B. Tabelin, T. Igarashi, M. Villacorte-Tabelin, I. Park, E. M. Opiso, M. Ito and N. Hiroyoshi, *Sci. Total Environ.*, 2018, **645**, 1522–1553.
3 M. W. Donner, B. Bicalho, C. Sinn and W. Shotyk, *Fuel*, 2018, **224**, 718–725.
4 C. B. Tabelin, I. Park, T. Phengsaart, S. Jeon, M. Villacorte-Tabelin, D. Alonzo, K. Yoo, M. Ito and N. Hiroyoshi, *Resour. Conserv. Recycl.*, 2021, **170**, 105610.
5 S. Vinayagam, K. Sathishkumar, R. Ayyamperumal, P. M. Natarajan, I. Ahmad, M. Saeed, N. M. Alabdallah and T. Sundaram, *Environ. Res.*, 2024, **240**, 117473.
6 Y. Li, X. Guo, H. Dong, X. Luo, X. Guan, X. Zhang and X. Xia, *Chem. Eng. J.*, 2018, **345**, 432–440.
7 M. Naga Jyothi, B. Ramaiah and S. M. Maliyekkal, *Measurement, Analysis and Remediation of Environmental Pollutants*, 2020, pp. 245–269.
8 S. Sharma and A. K. Sharma, *Selenium Contamination in Water*, 2021, pp.20–38.
9 I. Ali and V. Shrivastava, *J. Environ. Manage.*, 2021, **294**, 112926.
10 T. Li, H. Xu, Y. Zhang, H. Zhang, X. Hu, Y. Sun, X. Gu, J. Luo, D. Zhou and B. Gao, *Environ. Pollut.*, 2022, **299**, 118858.
11 J. Chen, X. Cheng and G. Sheng, *J. Radioanal. Nucl. Chem.*, 2023, **332**, 311–323.
12 K. L. Gullett, C. L. Ford, I. J. Garvey, T. J. Miller, C. A. Leahy, L. N. Awaitey, D. M. Hofmann, T. J. Woods and A. R. Fout, *J. Am. Chem. Soc.*, 2023, **145**, 20868–20873.
13 N. Bleiman and Y. G. Mishael, *J. Hazard. Mater.*, 2010, **183**, 590–595.
14 A. V. Kolliopoulos, J. P. Metters and C. E. Banks, *Anal. Methods*, 2013, **5**, 851–856.
15 M. Naderi, P. Puar, M. Zonouzi-Marand, D. P. Chivers, S. Niyogi and R. W. Kwong, *Sci. Total Environ.*, 2021, **767**, 144329.
16 B. S. Hoyos, F. Hernandez-Tenorio, A. M. Miranda, D. F. Villanueva-Mejía and A. A. Sáez, *Biology*, 2023, **12**, 703.
17 G. Bjørklund, M. Shanaida, R. Lysiuk, M. Butnariu, M. Peana, I. Sarac, O. Strus, K. Smetanina and S. Chirumbolo, *Molecules*, 2022, **27**, 7084.
18 X. G. Lei, G. F. Combs Jr, R. A. Sunde, J. S. Caton, J. D. Arthington and M. Z. Vatamaniuk, *Annu. Rev. Nutr.*, 2022, **42**, 337–375.
19 K. Sharma, A. Tayade, J. Singh and S. Walia, Functional Foods and Nutraceuticals: Bioactive Components, *Formulations and Innovations*, 2020, pp. 543–593.
20 R. L. Markley, K. H. Restori, B. Katkere, S. E. Sumner, M. J. Nicol, A. Tyryshkina, S. K. Nettleford, D. R. Williamson, D. E. Place and K. K. Dewan, *Front. Immunol.*, 2021, **12**, 701341.
21 J. Filip, Š. Vinter, E. Čechová and J. Sotolářová, *Analyst*, 2021, **146**, 6394–6415.
22 J. Vašková, L. Kočan, L. Vaško and P. Perjési, *Molecules*, 2023, **28**, 1447.
23 X. Phoon, E. L. Ander and J. A. Plant, *Pollutants, Human Health and the Environment: A Risk Based Approach*, 2012, vol. 53.
24 M. De Feudis, R. D'Amato, D. Businelli and M. Guiducci, *Sci. Total Environ.*, 2019, **659**, 131–139.
25 L. M. Walker, E. A. Karnaukh, F. Dewan and M. C. Buzzeo, *Electrochem. Commun.*, 2016, **69**, 28–31.
26 P. Devi, R. Jain, A. Thakur, M. Kumar, N. K. Labhsetwar, M. Nayak and P. Kumar, *TrAC, Trends Anal. Chem.*, 2017, **95**, 69–85.
27 D. H. Moon, D. G. Grubb and T. L. Reilly, *J. Hazard. Mater.*, 2009, **168**, 944–951.
28 R. Chawla, T. Filippini, R. Loomba, S. Cilloni, K. S. Dhillon and M. Vinceti, *Sci. Total Environ.*, 2020, **719**, 134541.
29 C. Chang, R. Yin, X. Wang, S. Shao, C. Chen and H. Zhang, *Sci. Total Environ.*, 2019, **669**, 83–90.
30 Z. Tan, W. Wu, N. Yin, M. Jia, X. Chen, Y. Bai, H. Wu, Z. Zhang and P. Li, *J. Food Compos. Anal.*, 2020, **94**, 103628.
31 A. R. dos Reis, H. El-Ramady, E. F. Santos, P. L. Gratão and L. Schomburg, *Selenium in Plants: Molecular, Physiological, Ecological and Evolutionary Aspects*, 2017, pp. 209–230.
32 D. Yadav, R. Jha, P. Kumar and P. Singh, *Selenium Contamination in Water*, 2021, pp. 91–114.
33 J. Das, S. Rawat, A. Maiti, L. Singh, D. Pradhan and P. Mohanty, *Sep. Purif. Technol.*, 2023, **306**, 122662.
34 J. Das, A. Rawat, L. Singh, A. Maiti, A. Bhatnagar and P. Mohanty, *ACS Appl. Eng. Mater.*, 2023, **1**, 2004–2017.
35 J. Das, A. Rawat, M. Chaudhary, A. Maiti and P. Mohanty, *J. Water Process Eng.*, 2024, **58**, 104823.
36 J. Das, A. Rawat, M. Chaudhary and P. Mohanty, *ACS Appl. Nano Mater.*, 2024, **7**, 1775–1785.
37 H. Devnani and C. Sharma, *Frontiers in Voltammetry*, 2022.

38 N. Tiwari, S. Chatterjee, K. Kaswan, J.-H. Chung, K.-P. Fan and Z.-H. Lin, *J. Electroanal. Chem.*, 2022, **907**, 116064.
39 I. Soni, A. Kumari, G. K. Jayaprakash, P. Naik and S. Rajendrachari, *Mater. Res. Express*, 2024, **11**, 012005.
40 P. R. Agrawal and R. Sharma, *Selenium Contamination in Water*, 2021, pp. 115–148.
41 S. Thakkar, L. F. Dumée, M. Gupta, B. R. Singh and W. Yang, *Water Res.*, 2021, **188**, 116538.
42 S. Rodrigo, J. Pizarro, K. Diaz, A Placencio, F. Godoy, E. Pino and F. Recio, *Sens. Actuators, B*, 2015, **220**, 263–269.
43 S. Tanaka, K. Sugawara and M. Taga, *Anal. Sci.*, 1990, **6**, 475–478.
44 M. Ashournia and A. Aliakbar, *J. Hazard. Mater.*, 2010, **174**, 788–794.
45 M. Ardalani, M. Shamsipur and A. Besharati-Seidani, *J. Electroanal. Chem.*, 2020, **879**, 114788.
46 D. Ayodhya, *Results Chem.*, 2023, **5**, 100874.
47 N. Dhiman, D. Pradhan and P. Mohanty, *Fuel*, 2022, **314**, 122722.
48 J. Wang, P. Yu, K. Kan, H. Lv, Z. Liu, B. Sun, X. Bai, J. Chen, Y. Zhang and K. Shi, *J. Chem. Eng.*, 2021, **420**, 130317.
49 M. Chaudhary, L. Singh, P. Rekha, V. C. Srivastava and P. Mohanty, *J. Chem. Eng.*, 2019, **378**, 122236.
50 N. Dhiman and P. Mohanty, *New J. Chem.*, 2019, **43**, 16670–16675.
51 S. P. Hageman, R. D. van der Weijden, J. Weijma and C. J. Buisman, *Water Res.*, 2013, **47**, 2118–2128.
52 R. Jain, A. Thakur, P. Kumar and D. Pooja, *Electrochim. Acta*, 2018, **290**, 291–302.
53 R. L. McCreery, *Chem. Rev.*, 2008, **108**, 2646–2687.
54 N. Baig, M. Sajid and T. A. Saleh, *TrAC, Trends Anal. Chem.*, 2019, **111**, 47–61.
55 A. Kumar, B. N. Mahanty, A. Rawat, R. Muhammad, R. K. Panigrahi, D. Pradhan and P. Mohanty, *Energy Fuels*, 2023, **37**, 6810–6823.
56 F. Marken, R. D. Webster, S. D. Bull and S. G. Davies, *J. Electroanal. Chem.*, 1997, **437**, 209–218.
57 Y. Lu, X. Liang, C. Niyungeko, J. Zhou, J. Xu and G. Tian, *Talanta*, 2018, **178**, 324–338.
58 Y. Jiao, Y. Zheng, M. Jaroniec and S. Z. Qiao, *Chem. Soc. Rev.*, 2015, **44**, 2060–2086.
59 A. Seifi, A. Afkhami and T. Madrakian, *J. Appl. Electrochem.*, 2022, **52**, 1513–1523.
60 C. L. Brosseau, A. Colina, J. V. Perales-Rondon, A. J. Wilson, P. B. Joshi, B. Ren and X. Wang, *Nat. Rev. Methods Primers*, 2023, **3**, 79.
61 S. E. Herrera-Rodríguez, N. Pacheco, T. Ayora-Talavera, S. Pech-Cohuo and J. C. Cuevas-Bernardino, *Stud. Nat. Prod. Chem.*, 2022, **73**, 221–264.
62 B. P. Chaplin, D. K. Hubler and J. Farrell, *Electrochim. Acta*, 2013, **89**, 122–131.